Three-dimensional elastic-plastic finite element analysis for wheel-rail rolling contact fatigue

Taek-Young Kim[1], Ho-Kyung Kim [*2]
[1]Graduate School, Seoul National University of Science and Technology,
172 Kongneung-dong, Nowon-ku, Seoul, 139-722, Korea
[2*] Dept. of Mech. & Automotive Eng. Seoul National University of Science and Technology
kimhk@seoultech.ac.kr

Abstract— Rolling contact fatigue of an urban railway wheel was analysed during its rolling FEM analysis was performed using 3D modelling of rail and wheel, in which the slope of the rail and nonlinear isotropic and kinematic hardening behavior of the rail and the wheel were considered. The maximum von Mises stress and contact pressure between the rail and wheel were determined under an axial load of 85 kN. The contact pressure distributions calculated using elastic Hertz theory and three-dimensional elastic–plastic stress analysis are compared. The maximum contact pressure of the wheel from the elastic-plastic FE method is slightly lower than the value from Hertz contact theory with elastic deformation. The rolling contact fatigue (RCF) of the wheel due to rolling contact was determined to be infinite by Dang Van criterion.

Keyword- Railway wheel, Rolling contact fatigue, Finite element method, Hertz contact theory, Dang Van criterion

I. INTRODUCTION

With the increasing demands of train traffic for heavier axle loads, greater traffic density, and higher train speeds, RCF failures of railway wheels become more serious. RCF can be surface or subsurface originated, mainly depending on the stress distribution and the material properties of the wheel. In order to understand and predict the fatigue and wear behavior of the wheel, an accurate stress analysis of the railway wheel is very important.

Two types of approaches are often used for stress analysis of the wheel, i.e. semi-analytical method and finite element method (FEM). Semi-analytical approach is generally based on elastic Hertz contact theory. It is simple but may provide reasonable rolling contact stress predictions. However, this method has a lower accuracy of the results for the rolling contact cases where large plastic deformation develops. FE approach is generally accurate when compared to semi-analytical methods. Wheel-rail contact analysis using FEM has been conducted by many researchers in various rail/wheel geometries under different conditions to evaluate stress distributions of the contact regions. From the analysis, plastic deformation, crack initiation, vehicle dynamics and wear can be analyzed. Most of the FEM conducted so far were restricted to two-dimensional rolling contact [1]-[4]. Three-dimensional elastic–plastic stress analysis of rolling contact of railway wheel using the FEM is very limited in the literature. Proper simulation provides clear understanding of a detailed knowledge of physical interaction between wheel and rail.

In this study, three-dimensional elastic–plastic stress analysis of rolling contact of railway wheel is conducted on a 3D wheel-rail model. Then, the contact pressure distributions calculated using elastic Hertz theory and three-dimensional elastic–plastic stress analysis are compared. Finally, the FEM results are analyzed adopting Dang Van criterion [5] for RCF life assessment of the railway wheels.

II. HERTZ CONTACT THEORY FOR THE WHEEL AND RAIL

When a wheel and a rail are brought into contact under the action of the static wheel load, the contact area and the pressure distribution are usually determined using the Hertz theory [6]. In Hertz contact theory, no plastic deformation in the contact patch is assumed, and the radii of the curvature of wheel and rail profiles in the contact patch are assumed to be constant. According to Hertz theory, the normal pressure is distributed as an ellipsoid over the elliptic contact area. The ellipsoidal normal contact pressure distribution $p(x,y)$ is expressed by

$$p(x,y) = \frac{3W}{2\pi ab}\sqrt{1-(\frac{x}{a})^2-(\frac{y}{b})^2} \quad (1)$$

Here, a and b are the half width of the contact area in the longitudinal x and lateral y directions, respectively, while W is the total normal contact force, as shown in Fig.1. The parameters are given by

$$a = m\sqrt[3]{\frac{3\pi}{4}\frac{W(k_1+k_2)}{(A+B)}}\,, \tag{2}$$

$$b = n\sqrt[3]{\frac{3\pi}{4}\frac{W(k_1+k_2)}{(A+B)}}\,. \tag{3}$$

The modulus k_1 and k_2 are given by;

$$k_1 = \frac{1-\nu_1^2}{\pi E_1}, \tag{4}$$

$$k_2 = \frac{1-\nu_2^2}{\pi E_2}, \tag{5}$$

$$A+B = \frac{1}{2}\left(\frac{1}{R_1}+\frac{1}{R_1'}+\frac{1}{R_2}+\frac{1}{R_2'}\right), \tag{6}$$

$$A-B = \frac{1}{2}\sqrt{\left(\frac{1}{R_1}-\frac{1}{R_1'}\right)^2+\left(\frac{1}{R_2}-\frac{1}{R_2'}\right)^2+2\left(\frac{1}{R_1}-\frac{1}{R_1'}\right)\left(\frac{1}{R_2}-\frac{1}{R_2'}\right)\cos(2\psi)}\,, \tag{7}$$

$$\cos(\theta) = \frac{B-A}{A+B}\,, \tag{8}$$

where R_1 and R_2 are the wheel nominal rolling radius and the rail lateral section curve radius, respectively. Also, E_1 and E_2 are the Young's moduli of the wheel and rail materials, respectively, and ν_1 and ν_2 are the Poisson's ratios of the wheel and rail materials, respectively. The angle of ψ is between the radius of the wheel and rail and θ is the angle between the principal axes. The values of *m* and *n* for the angle θ are given in the table [6].

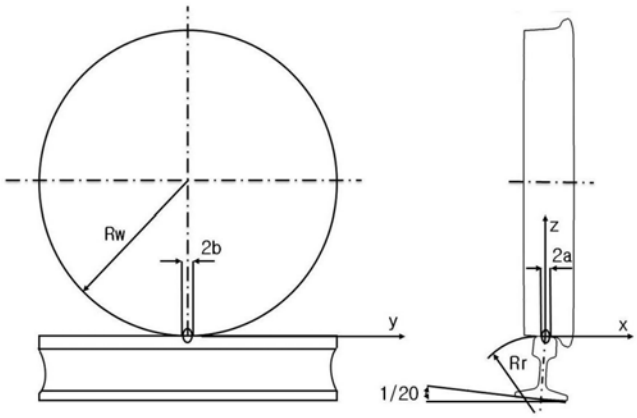

Fig. 1. Wheel-rail contact area

These parameters of the wheel and rail are assumed to be identical since steels are used for both rail and wheel, and most steels have practically identical elasticity modulus and Poisson's ratio values. The maximum normal contact pressure and the contact lengths *a* and *b*. $E_1 = E_2 = 210$ GPa, and $\nu_1 = \nu_2 = 0.3$ are used.

Consider the contact of a wheel with a cylindrical rim of radius R_1 = 430 mm and a rail with the radius of the head R_2 = 300 mm. We find, substituting $1/R_1' = 1/R_2' = 0$ for the wheel and rail and the angle ψ between the radius of the wheel and rail is $\psi = \pi/2$ into Eqs. (6) and (7),

A + B = 0.00283, B - A = 0.005. The angle θ can be calculated as 79.7°. Then, by interpolation, the values of *m* and *n* can be determined from the table [6] as follows: *m* =1.128, *n* = 0.893.

Substituting in Eqs. (2) and (3), the values of *a* and *b* can be calculated for W = 85 kN as follows: a = 6.54 mm, b = 5.18 mm. Finally, the maximum pressure at the center is 1198.1 MPa, which is above yield strength of the wheel steel.

It is clear that the Hertz contact theory involves rough assumptions and is not suitable for application to the railway wheel and rail contact situation. For example, for contacts near the gauge corner of the crossing rail, there is a significant variation of the wheel and rail profile curvatures within the contact area, and the

dimensions of the contact area may not be small compared to the radii of curvature of the contacting surfaces. The railway wheel actually runs on the rail mounted on the ground with a constant angle. A non-elliptical contact area may result when contact occurs close to the gauge corner. Thus, the Hertz theory is not valid for the real situation of wheel and rail contact. Therefore, analysis is needed in which the rail mounting angle and plastic-elastic deformation behavior of the wheel steel is considered through 3D contact analysis of rail–wheel.

III. FEA PROCEDURE

A commonly used 860 mm diameter wheel and the corresponding rail geometries (UIC50 model) were created using Pro-Engineering CAD software and the assembly of the symmetrical model comprising wheel and rail is presented in Fig. 2. This 3D model geometry was transferred to the HyperMesh software and meshed with C3D6 6-noded wedge elements and C6D8 8-noded brick elements as shown in Fig. 2. The mesh at contact locations was refined very well with a minimum element length of 1 mm to accurately model the contact region as shown in Fig. 2.

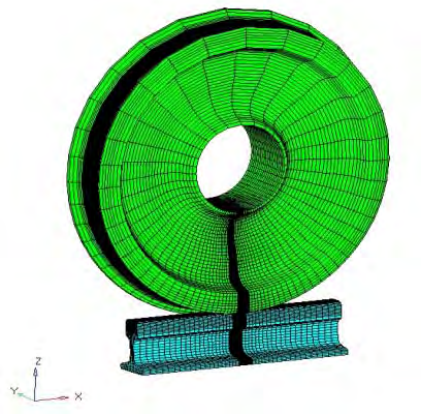

Fig. 2. Wheel/rail contact model for FE analysis

Contact between rail and wheel was modeled using ABAQUS Master elements placed on the wheels and ABAQUS Slave elements placed on the rails. FE model mesh (wheel + rail) was obtained with a total of 215,742 elements and 229,231 nodes. Under the total vertical load of 680 kN (wagon dead-weight + pay load) per total of 8 wheels in a wagon, resulting to 85 kN per wheel was applied. Wheels were assumed to operate on a flat, straight path; therefore, lateral loads to the system were ignored. The rotational effect of the wheels was also neglected. The friction coefficient, μ= 0 and 0.2 was used in the FE analysis. The rail and wheel material properties were assumed to be the same, and a non-linear kinematic hardening elastic–plastic material model was used. Boundary and loading condition were applied to the 1/4 FE model. Symmetry boundary conditions were applied at cut surfaces of the 1/4 rail–wheel model at the cut normal directions. The rail was fixed at traverse locations in all directions to prevent rigid body motion of the whole system. The mounting slope of the rail on the ground (1/20 radian) is taken into consideration for contact analysis of wheel-rail.

IV. EVALUATION OF THE MECHANICAL PROPERTIES FOR THE WHEEL STEEL

Specimens were extracted from the wheel tread in order to evaluate the material parameters, including fatigue properties. Tension–compression high-cycle fatigue and high-cycle torsional fatigue experiments were performed. The stress–strain curve from a tensile test is presented in Fig. 3. Fig. 3 shows the engineering and true stress-strain curves of a sample from the wheel tread. As seen in Fig. 3, the engineering ultimate tensile and yield strengths were 1027.7 MPa and 626.7 MPa, respectively. Elongation was 40.4%, and the true fracture strength was 1319.5 MPa.

Fig. 4 shows the relationship between the maximum principal stress amplitude and the fatigue life from uniaxial and biaxial torsional fatigue tests. From Fig. 4, the uniaxial (σ_e) and biaxial torsional (τ_e) fatigue limits were 422.5 MPa and 265.0 MPa, respectively. This figure shows that the uniaxial specimen had a longer fatigue life than the biaxial torsional specimen under the same maximum principal stress. The fatigue limit found in the uniaxial fatigue test was 67% of the tensile strength, which is relatively high, compared to about 50% of typical steels. The ratio of the uniaxial fatigue limit against the biaxial torsional fatigue strength τ_e/σ_e was 0.63, and this value is almost the same as 0.6, which is the value for typical ductile materials. For brittle materials, the τ_e/σ_e ratio is typically known to be about 0.8 or higher [7].

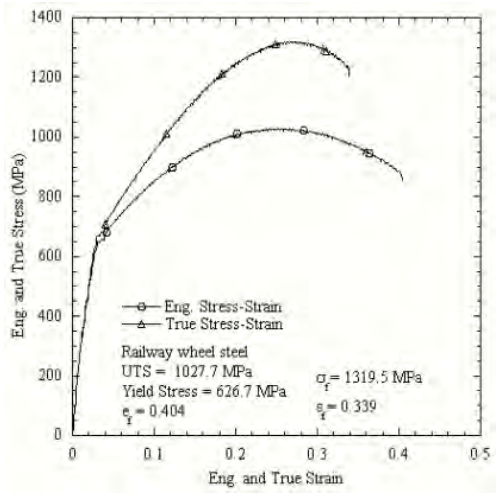

Fig. 3. Engineering and true stress-strain curves of railway wheel steel

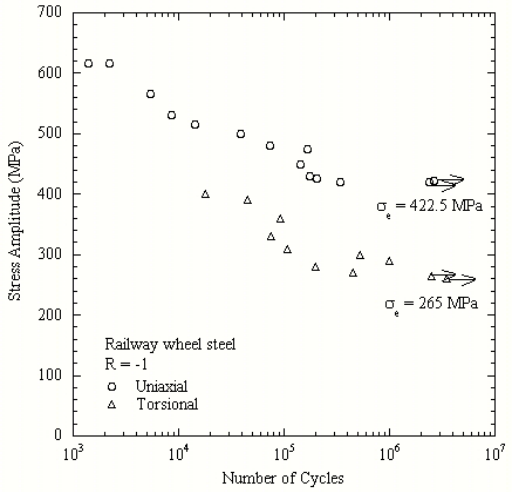

Fig. 4. Stress amplitude against number of cycles for uniaxial and biaxial torsional fatigue tests

In general, a Dang Van equation [5], like Equation (9) below, is applied under damaged conditions by high cycle fatigue, which is equivalent to elastic shakedown, as another method to predict the fatigue life by rolling contact.

$$\left|\tau_a(t) \pm \alpha_{DV}\sigma_h(t)\right| \le \tau_e \tag{9}$$

Here, $\tau_a(t)$ is the maximum shear strength amplitude, $\sigma_h(t)$ is the hydrostatic pressure, α_{DV} is the material constant, and τ_e is the shear fatigue limit. Accordingly, if the sum of the shear stress amplitude and the hydrostatic pressure is greater than the fatigue limit of the material, fatigue is accumulated, leading to fatigue damage. At this time, the material constant of Dang Van, α_{DV}, is a very important material constant related to the fatigue limit ratio at the biaxial shear and uniaxial load conditions. α_{DV} defined as shown in Equation (10):

$$\alpha_{DV} = 3\left(\frac{\tau_e}{\sigma_e} - \frac{1}{2}\right) \tag{10}$$

For this material, it was determined to be $\alpha_{DV} = \frac{3\tau_e}{\sigma_e} - \frac{3}{2} = \frac{3\times 265}{422.5} - 1.5 = 0.38$. In some studies on railway steel wheel, it has been reported as α_{DV} = 0.99 ~ 0.94 [5]. The mechanical and fatigue properties of the railway steel wheel of this study are shown in Table 1.

Table 1 Mechanical and fatigue properties of the railway wheel steel

UTS (MPa)	YS (MPa)	Elong. (%)	σ_e (MPa)	τ_e (MPa)	α_{DV}
1027.7	626.7	40.4	422.5	265.0	0.38

V. RESULTS AND DISCUSSIONS

5.1 Stress distribution on the wheel

The final FE model was run at a friction coefficient μ of 0 and 0.2 between the wheel and the rail and post-processed successfully to visualize stress and strain levels. In Fig. 5(a), von Mises stress is plotted for the wheel contacting the rail at μ of 0.2. The maximum stress was 656.9 MPa inside of the outer surface, above the yield strength (=626.7 MPa) for wheel steel. This figure reveals that the stress level at the spoke of the wheel is much lower than that of the contact region. Fig. 5(b) shows the detailed von Mises stress distribution at the contact region for Fig. 5(a). As seen in the figure, the maximum stress of 656.9 MPa was found at 4.05 mm inside of the outer surface. The maximum contact pressure between the wheel and the rail at μ of 0 and 0.2 were 1111.4 MPa, 1092.4 MPa, respectively, indicating that there was little effect of the friction coefficient on contact pressure. This fact is consistent with the result obtained by Guo et al. [8]. They reported that the stress level and its consequent effect on fatigue damage with the increment of the friction coefficient are not significant, which they investigated through FEM analysis on rolling contact of the wheel.

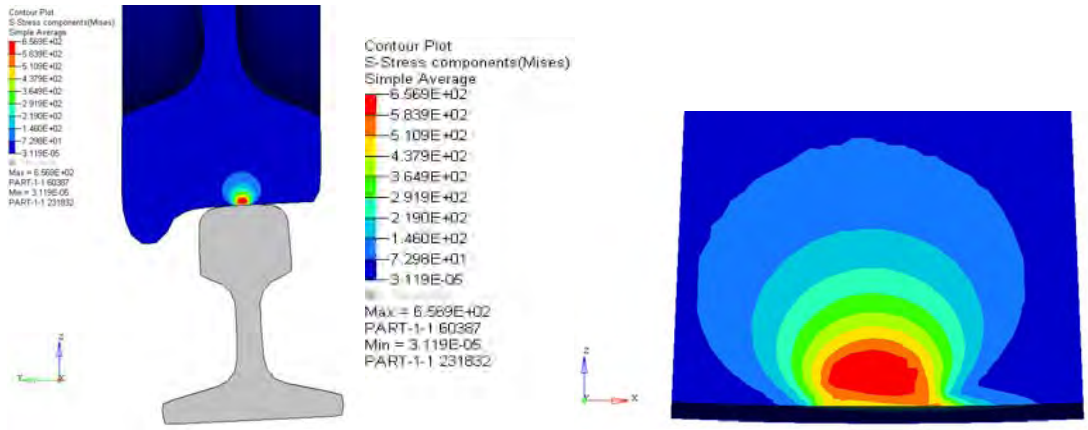

(a) (b)

Fig. 5. (a) Von Mises stress distribution and (b) detailed distribution of the wheel-rail contact at μ = 0.2.

Fig. 6(a) shows the 3D distribution of wheel-rail contact pressure under an axle load. This figure reveals that the maximum pressure of the wheel is 1111.4 MPa, which is about 7 percent lower than the value (=1198.1 MPa) from Hertz contact theory with elastic deformation. The difference of maximum contact pressure between the FE method and calculation by the elastic Hertz theory might be due to an assumption between the elastic Hertz theory and the elastic-plastic finite element method. Moreover, the 3D FEM model considers the inclination angle between rail and ground, whereas the Hertz theory does not consider this.

Fig. 6(b) shows the contact pressure distribution on the contact area in 2D, indicating that the distribution area is elliptical in shape and is symmetric with respect to the *x* axis corresponding to the rail travel direction. The shape of the contact area is similar to the result obtained by other research [9] adopting 3D modeling and elastic-plastic deformation behavior. The half width of the contact area in the *x* and *y* directions, respectively, are a = 7.5 mm and b = 6.3 mm, based on the results of 3D FEM analysis. These values are slightly larger than those from the Hertz theory (a = 6.54 mm, b = 5.18 mm).

Fig. 7 shows a comparison of contact pressure distribution on the contact surface in the longitudinal direction determined by the Hertz theory and FEM analysis with μ = 0. This figure reveals that the result obtained from 3D FEM adopting elastic-plastic deformation behavior in the contact zone is similar to that obtained from the Hertz theory based on elastic deformation behavior. This indicates that this FEM analysis was conducted appropriately. In addition, the maximum contact pressure observed in the 3D FEM analysis is slightly lower than that obtained by the Hertz theory due to increased contact area with plastic deformation.

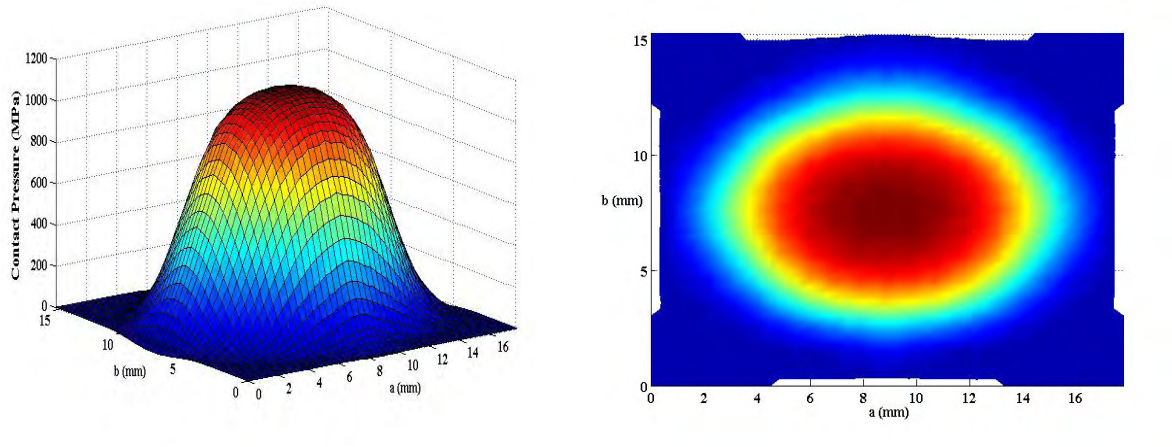

(a) (b)

Fig. 6. (a) Normal contact pressure 3D distribution on the contact surface, and (b) contact pressure distribution on the contact area determined by FEM analysis with μ = 0.

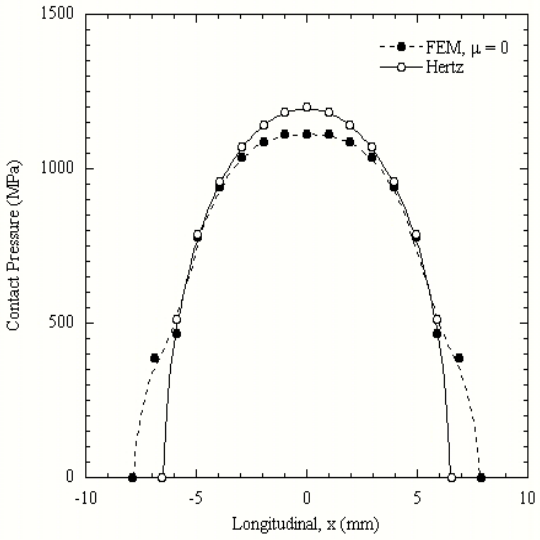

Fig. 7. Comparison of contact pressure distribution on the contact surface in longitudinal direction determined by Hertz theory and FEM analysis with μ = 0.

5.2 Rolling contact fatigue life analysis

In the present investigation, RCF life of the railway wheel was assessed using the Dang Van criterion [5]. The criterion was evaluated against 3D elastic–plastic FE simulations of the wheel. The shear stress amplitude and hydrostatic stress of the critical location of the wheel during its one revolution on the rail were plotted in Fig. 8, in the $\tau_a(t)-\sigma_h(t)$ curves, adopting Dang Van equation (9). Here, straight line of slope α_{DV} passes through the vertex of the curve representing τ_e / α_{DV} value. The critical location corresponds to the place with maximum contact pressure. The hydrostatic stress was determined with the relation $\sigma_h = (\sigma_1 + \sigma_2 + \sigma_3)/3$. In this curve, we adopted α_{DV} =0.38 for this wheel steel. Table 2 summarized the FE analysis results for Dang Van criterion. Here, (x, y, z) coordinates are in rail traveling direction, rail transverse direction and wheel depth direction, respectively, in mm unit. And the reference point (0, 0, 0) is corresponding to the center of the wheel and rail contact point. The shear and hydrostatic stresses data of the critical location of the wheel are within the experimental limit, as shown in Fig. 8, indicating that no cracks will initiate during rolling for the railway wheel of this study.

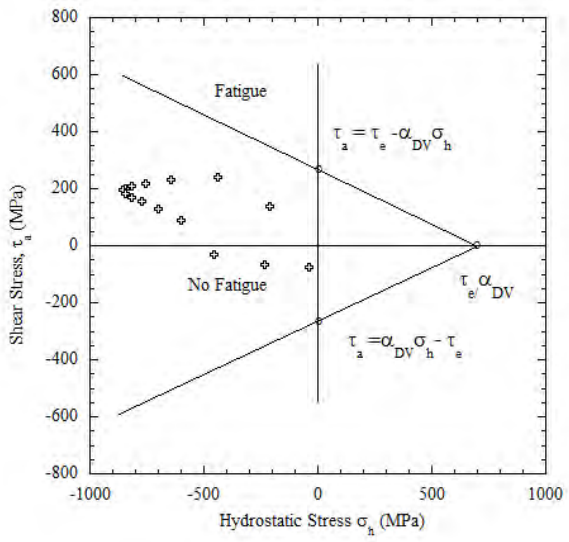

Fig. 8. The Dang Van diagram for the rolling contact of the wheel

Table 2 FE analysis results for Dang Van criterion

x, y, z (mm)	τ_a (MPa)				σ_h (MPa)
		σ_1	σ_2	σ_3	
-6.90, 0, 0	139.9	6.5	-238.0	-396.2	-209.2
-5.91, 0, 0	240.6	-204.0	-399.0	-714.1	-439.0
-4.92, 0, 0	231.8	-434.1	-564.5	-928.6	-642.4
-3.94, 0, 0	219.8	-558.7	-670.2	-1038.3	-755.7
-2.95, 0, 0	211.3	-625.0	-728.1	-1096.1	-816.4
-1.97, 0, 0	202.2	-655.9	-757.2	-1122.9	-845.3
-0.99, 0, 0	193.7	-652.1	-779.1	-1130.2	-853.8
0, 0, 0	181.4	-637.9	-779.1	-1122.1	-846.3
0.99, 0, 0	170.2	-603.6	-749.7	-1101.3	-818.2
1.97, 0, 0	154.2	-534.1	-719.3	-1057.4	-770.2
2.95, 0, 0	127.6	-445.8	-666.9	-990.4	-701.0
3.94, 0, 0	89.8	-325.7	-587.6	-889.0	-600.8
4.92, 0, 0	-31.3	-151.2	-478.1	-729.0	-452.8
5.91, 0, 0	-67.3	106.4	-318.5	-486.8	-233.0
6.90, 0, 0	-76.8	266.2	-138.1	-240.8	-37.6

VI. CONCLUSION

The rolling contact fatigue of an urban train wheel was analysed during its rolling. FEM analysis was performed using 3D modelling of rail and wheel, in which the slope of the rail and nonlinear isotropic and kinematic hardening behavior of the rail and the wheel were considered. The maximum von Mises stress was 656.9 MPa under an axial load of 85 kN with the friction coefficient of 0. The maximum contact pressure of the wheel from the elastic-plastic FE method is about 7 percent lower than the value from Hertz contact theory with elastic deformation. Based on the results of 3D FEM analysis, the maximum radius (=a) of the contact area is 7.50 mm, which is about 13 percent larger than value from Hertz contact theory. The maximum contact pressure between the wheel and the rail at μ of 0 and 0.2 were 1111.4 MPa, 1092.4 MPa, respectively, indicating there was little effect of the friction coefficient on contact pressure. The fatigue life of the wheel during its one revolution on the rail due to rolling contact was determined to be infinite by Dang Van criterion.

ACKNOWLEDGMENT

This study was financially supported by Seoul National University of Science & Technology.

REFERENCES

[1] M. Taraf, E.H.Zahaf, O.Oussouaddi, and A.Zeghloul, “Numerical analysis for predicting the rolling contact fatigue crack initiation in a railway wheel steel,” Tribology Int. vol. 43, pp. 585-593, 2010.

[2] L. Wu, Z. Wen, W. Li, and X. Jin, “Thermo-elastic–plastic finite element analysis of wheel/rail sliding contact,” Wear, vol. 271, pp. 437–443, 2011.

[3] J.W. Ringsberg, M. Loo-Morrey, B.L. Josefson, A. Kapoor, and J.H. Beynon, “Prediction of fatigue crack initiation for rolling contact fatigue,” Int. J. Fatigue, vol. 22, pp. 205–215, 2000.

[4] D. Canadinc, H. Sehitoglu, and K. Verzal, “Analysis of surface crack growth under rolling contact fatigue,” Int. J. Fatigue, vol. 30, pp. 1678–1689, 2008.

[5] K. Dan Van, B. Griveau, and O. Message, “On a new multiaxial fatigue limit criterion: Theory and Application, in Biaxial and Multiaxial Fatigue,” European Group on Fracture, EGF Publication 3, Mech. Eng. Publ., London, pp. 479-496, 1989.

[6] S.P. Timoshenko and J.N. Goodier, *Theory of Elasticity*, 3rd ed. McGraw-Hill Co. pp. 414-418, 1970.

[7] A Bernasconi, M. Filippini, S. Foletti, and D. Vaudo, “Multiaxial fatigue of a railway wheel steel under non-proportional loading,” Int. J Fatigue. vol. 28, no.5-6, pp. 663-672, 2006.

[8] Y.B. Guo and M.E. Barkey, “Modeling of rolling contact fatigue for hard machined components with process-induced residual stress,” Int. J. Fatigue, vol. 26, pp. 605-613, 2004.

[9] M. Wiest, E. Kassa, W. Daves, J.C.O. Nielsen, and H. Ossberger, “Assessment of methods for calculating contact pressure in wheel-rail/switch contact,” Wear, vol. 265, pp. 1439-1445, 2008.